

updated September 6, 2018

# Central Masses and Broad-Line Region Sizes of Active Galactic Nuclei: I. Comparing the Photoionization and Reverberation Techniques

A. Wandel<sup>1,2</sup>, B.M. Peterson<sup>3</sup>, and M.A. Malkan<sup>1</sup>

## ABSTRACT

The masses and emission-line region sizes of AGNs can be measured by “reverberation-mapping” techniques and we use these results to calibrate similar determinations made by photoionization models of the AGN line-emitting regions. Reverberation mapping uses the light travel-time delayed emission-line response to continuum variations to determine the size and kinematics of the emission-line region. We compile a sample of 17 Seyfert 1 galaxies and 2 quasars with reliable reverberation and spectroscopy data, twice the number available previously. The data provide strong evidence that the BLR size (as measured by the lag of the emission-line luminosity after changes in the continuum) and the emission-line width measure directly the central mass: the virial assumption is tested with long-term UV and optical monitoring data on NGC 5548. Two methods are used to estimate the distance of the broad emission-line region (BLR) from the ionizing source: the photoionization method (which is available for many AGNs but has large intrinsic uncertainties), and the reverberation method (which gives very reliable distances, but is available for only a few objects). The distance estimate is combined with the velocity dispersion, derived from the broad  $H\beta$  line width (in the photoionization method) or from the variable part (RMS) of the line profile, in the reverberation -RMS method, to estimate the virial mass. Comparing the central masses calculated with the reverberation -RMS method to those calculated using a photoionization model, we find a highly significant, nearly linear correlation. This provides a calibration of the photoionization method on the objects with presently available reverberation data, which should enable mass estimates for all AGNs with measured  $H\beta$  line width. We find that the correlation between the masses is significantly better than the correlation between the corresponding BLR sizes calculated by the two methods, which further supports the conclusion that both methods measure the mass of the central black hole. Comparing the BLR sizes given

---

<sup>1</sup>Astronomy Department, University of California, Los Angeles, CA 90095-1562, E-mail: [wandel@astro.ucla.edu](mailto:wandel@astro.ucla.edu), [malkan@astro.ucla.edu](mailto:malkan@astro.ucla.edu)

<sup>2</sup>Permanent address: Racah Institute, The Hebrew University, Jerusalem 91904, Israel

<sup>3</sup>Department of Astronomy, The Ohio State University, 174 West 18th Avenue, Columbus, OH 43210-1106, E-mail: [peterson@astronomy.ohio-state.edu](mailto:peterson@astronomy.ohio-state.edu)

by the two methods also enables us to estimate the ionizing EUV luminosity  $L_{ion}$  which is directly unobservable. Typically it is ten times the monochromatic luminosity at 5100 Å ( $L_v$ ). The Eddington ratio for the objects in our sample is in the range  $L_v/L_{Edd} \sim 0.001 - 0.03$  and  $L_{ion}/L_{Edd} \approx 0.01 - 0.3$ .

*Subject headings:* galaxies: active — galaxies: nuclei — galaxies: Seyfert — quasars: general — black holes — emission-lines — photoionization

## 1. Introduction

The most fundamental characteristics of the quasar–AGN powerhouse, the central mass and structure, are not well understood. The broad emission lines probably provide the best probe of these characteristics because the broad-line region (BLR) is the only part of the AGN structure where we can measure accurate Doppler motions of gas on appropriate physical scales. In particular, assuming the line-emitting matter is gravitationally bound, and hence has a near-Keplerian velocity dispersion, it is possible to estimate the virial central mass.

The virial assumption  $v \propto r^{-1/2}$  has been directly tested using preliminary data for only NGC 5548 (Krolik et al. 1991; Rokaki, Collin-Souffrin, & Magnan 1993). These works demonstrated the case for a Keplerian velocity dispersion in the line-width/time-delay data, for several broad lines in two different BLR models. The presently available data support these preliminary results and provide strong evidence for Keplerian velocity dispersion in NGC 5548 (Peterson & Wandel 1999; cf. section 4). Although the virial assumption of Keplerian motion is essential for estimating the mass from the BLR observed properties, the estimate may be approximately correct also for models in which the line-emitting gas is not bound, such as wind or radiation-pressure induced velocities, because the emissivity in a diverging flow decreases rapidly, and most of the emission would occur near the base of the flow, when the velocity is still close to the escape velocity, which is of the order of the Keplerian velocity (e.g. Murray et al. 1998).

The main challenges in estimating the virial mass from the emission-line data are to obtain a reliable estimate of the size of the BLR, and to relate correctly the line profile to the velocity dispersion in that gas. Reliable BLR size measurements are now possible through reverberation mapping techniques (Blandford & McKee 1982, recently reviewed by Netzer & Peterson 1997). The continuum/emission-line cross-correlation function measures the responsivity-weighted radius of the BLR (Koratkar & Gaskell 1991). The spectra can be combined to form the mean spectrum and the RMS spectrum, which identifies the variable part of the emission line. This method can be used only for a limited number of AGN, because it can be applied only to variable sources and requires well-sampled spectra over time scales of months to years. Such data are difficult to obtain and exist for fewer than two dozen AGN, mostly low- to moderate-luminosity Seyfert galaxies.

An alternative method of estimating the virial mass is based on estimating the BLR distance

from the central mass using photoionization theory (Netzer 1990), and the emission-line width as an indicator of the velocity dispersion. This method only assumes the line-emitting gas is gravitationally bound, but does not depend on the specific BLR geometry or model, so it could apply to cloud models as well as disk models (e.g., Rokaki, Boisson, & Collin-Souffrin 1992).

In its simplest version, the line ratios are used to determine the conditions in the ionized line-emitting gas, in particular the density and the ionization parameter  $U$  (the number of ionizing photons per electron)

$$U = \frac{Q}{4\pi r^2 n_e c} = \frac{L_{ion}}{4\pi r^2 \bar{E} n_e c}, \quad (1)$$

where

$$Q = \int_{1\text{Ryd}} \frac{L_\nu}{h\nu} d\nu$$

is the number of ionizing photons,  $L_{ion}$  is the ionizing luminosity and  $\bar{E} = L_{ion}/Q$  is the average energy of an ionizing photon. With an estimate of the luminosity of ionizing spectrum, (Mathews & Ferland 1987; Bechtold et al. 1987; Zheng et al. 1997; Laor et al. 1998) the eq. 1 can be inverted to give the distance of the ionized gas from the continuum source. Wandel (1997) has demonstrated that the BLR sizes derived even by the basic photoionization method are in good agreement with the reverberation sizes. He also showed that using soft X-ray data to obtain a better estimate of the ionizing flux can significantly improve the correlation, quantifying the error introduced by the uncertainty in the ionization parameter  $U$  and the density  $n_e$ .

A recent compilation of the available objects with reverberation data (Kaspi et al. 1997) shows that the BLR size scales roughly as the square root of the luminosity, which agrees with the intuitive prediction of the basic photoionization method, assuming that BLR in different AGN have similar values (or a narrow, luminosity-independent distribution) of the ionization parameter and density.

In contrast to the reverberation method, the photoionization method is indirect and the BLR sizes derived are subject to many intrinsic uncertainties. The line emission is probably extended in radius, and includes emission from gas with a range of densities, so that single-zone models oversimplify the real situation. While simple photoionization models may not be trusted for estimating BLR parameters, it should be possible to calibrate the photoionization method using reverberation results (Wandel 1998).

Since the photoionization method can be used for any AGN, even with low-resolution spectroscopy (and even with a single observation), it has enormous potential. If the method can be calibrated, as we attempt to in this work, it could give virial masses of a large number of AGN, virtually all of those having reasonably well-established  $H\beta$  line widths and UV line ratios. A growing number of high-redshift quasars are also now being observed in the  $H\beta$  line with good infrared spectroscopy, which we will also use (McIntosh et al. 1998). Such a calibration will provide us with a powerful tool to determine reliable BLR sizes and virial masses of a large number of AGN, and improve our understanding of the  $M/L$  relation and the structure of the BLR.

In the present work we investigate whether or not such a calibration is feasible, using all the presently available reverberation and emission-line variability data.

An important feature of this paper is that we present a sample of AGN that have been analyzed in a consistent fashion, providing reliable estimates (to within basically geometrical factors of order unity) of AGN black hole masses. The method of estimating virial masses is superior to what has been done previously, as we use the scale length from reverberation techniques and only the variable part of the emission line to obtain a Doppler width by measuring the line width in the rms rather than the mean spectrum. The sample analyzed here is about twice as large as any previously discussed sample.

In the next section we describe the photoionization method. Section 3 describes the reverberation - RMS method and data. In section 4, we consider the multi-year observations of NGC 5548. Sections 5-6 give the correlation results for the central masses and the BLR sizes, section 7 discusses the ionizing luminosity and Eddington ratio estimates, and section 8 discusses our result and the uncertainties associated with the sample selection, with the reverberation methods and of the photoionization method.

## 2. The Basic Photoionization Method

As a preliminary test we use the calibration of the ionization-parameter method in its most basic form — the BLR modeled by a single thin shell, with an average value of  $Un_e$  assumed for all objects. Combining the definition of the ionization parameter with the assumption of virialized velocity dispersion gives the simplest version of the photoionization virial mass estimate:

$$M_{ph} \approx \frac{R_{ph} v^2}{G} = K \left( \frac{L_{ion}}{Un_e \bar{E}} \right)^{1/2} (v_{FWHM})^2 \quad (2)$$

where  $K = f_k G^{-1} (4\pi c)^{-1/2}$  and  $f_k$  is the factor relating the effective velocity dispersion to the projected radial velocity deduced from the emission-line Doppler broadening, and  $R_{ph}$  is the radius derived from eq. 1. Relating the velocity dispersion to the FWHM we assume  $\langle v^2 \rangle = \frac{3}{4} v_{FWHM}^2$ , so  $f_k = 3/4$  (Netzer 1990).

Since we intend to find the normalization factor with respect to the reverberation-rms direct method, we do not have to worry about the precise factors, but keeping the constants can give an estimate of the effective values of the physical parameters. The size of the BLR is then derived from eq. (1). As we do not know the ionizing luminosity, we need to estimate it. In this work, as a zero-order estimate we assume it is proportional to the visible luminosity, and try to determine the sample average of the proportionality constant by the calibration. A priori it is reasonable that this assumption would contribute to the errors, because individual AGN may have different  $L_{ion}/L_V$  ratios. However, as we see below, apparently this is not the case, at least for the sample at hand. More elaborate estimates of the ionizing continuum may be attempted by using near UV

(Zheng et al. 1997) or soft X-ray (Wandel 1997; Laor 1998) data, but it is not clear how much these improve the estimate of  $L_{ion}$ , because we do not know the shape of the EUV, and these data are also not available for many AGN; our intention is to develop an “affordable” method, applicable to as many AGN as possible. Finally, the spectral correction enters as a square root, which reduces the eventual errors contributed to the mass estimate. Relating the ionizing luminosity to some measured luminosity  $L$  eq. (1) gives

$$R_{ph} \approx 13 \left( \frac{f_L L_{44}}{U n_{10} \bar{E}_1} \right)^{1/2} \text{ lt - days}, \quad (3)$$

where  $L_{44} = L/10^{44} \text{ erg s}^{-1}$  and  $f_L = L_{ion}/L$  is the factor relating the observed luminosity  $L$  to the ionizing luminosity,  $\bar{E}_1 = \bar{E}/1 \text{ Ryd}$  which gives

$$M_{ph} \approx (2.8 \cdot 10^6 M_\odot) f \left( \frac{L_{44}}{U n_{10}} \right)^{1/2} v_3^2, \quad (4)$$

where  $f = f_k f_L^{1/2} \bar{E}_1^{-1/2}$  and  $v_3 = v_{\text{FWHM}}/10^3 \text{ km s}^{-1}$ .

As a first approximation, we assume the ionizing luminosity is proportional to the visual luminosity  $L_V \approx \nu L_\nu(5100 \text{ \AA})$ . For our purpose this is equivalent to assuming that the ionizing luminosity is proportional to  $\nu L_\nu$ .

As discussed in section 7 below, comparing the reverberation and photoionization BLR sizes can be used to estimate  $f_L$ .

### 3. Reverberation-RMS Masses

#### 3.1. The Method

The reverberation BLR sizes and the masses are derived by Peterson et al. (1998a)<sup>4</sup>. The size of the BLR is measured by observing the light travel-time delayed response of the emission line to continuum variations. The relationship between the light curve  $L(t)$  and the emission-line intensity  $I(t)$  is assumed to be

$$I(t) = \int \Psi(\tau) L(t - \tau) d\tau,$$

where  $\Psi(\tau)$  is the transfer function (Blandford & McKee 1982). The transfer function depends on the BLR geometry, the viewing angle and the line emissivity. The cross-correlation of the continuum and emission-line light curves is given by

$$CC(\tau) = \int \Psi(\tau') AC(\tau' - \tau) d\tau',$$

---

<sup>4</sup>On account of several typesetting errors in the original paper, the values for masses are superseded by the masses given in Table 2 below.

where AC is the continuum autocorrelation function (Penston 1991). It can be shown (Koratkar & Gaskell 1991) that the centroid of the cross-correlation function,  $\tau_{cent}$ , gives the size  $c\tau_{cent}$  associated with the emissivity-weighted mean radius for the emission region of a particular emission-line.

The root-mean-square (RMS) spectrum defined as

$$\sigma(\lambda) = \left[ (N - 1)^{-1} \sum_i^N (F_i(\lambda) - \bar{F}(\lambda))^2 \right]^{1/2} \quad (5)$$

where  $N$  is the number of spectra and  $\bar{F}$  is the average spectrum. The RMS spectrum measures the variations about the mean, automatically excluding constant features such as narrow emission lines, Galactic absorption and constant continuum and broad line features. The RMS H $\beta$  emission-line profile gives the velocity dispersion in the variable part of the gas, the one which is used to calculate the BLR size.

The line width and the BLR size may be combined to yield the virial "reverberation" mass estimate (equivalent to eq. 4)

$$M_{rev} \approx (1.45 \times 10^5 M_{\odot}) \left( \frac{c\tau}{\text{light - days}} \right) v_{rms,3}^2, \quad (6)$$

where  $v_{rms,3} = v_{FWHM}(rms)/10^3 \text{ km s}^{-1}$ .

### 3.2. The Data

Our sample consists of 19 objects, 17 Seyfert 1 galaxies and 2 quasars. This is the most complete compilation to date of AGNs for which reverberation data are available. The sample will be described in a separate paper, and in this contribution we consider only ground-based optical data. These data are drawn from the following sources:

1. **The Ohio State AGN Monitoring Program.** A program of approximately weekly observations of the H $\beta$  spectral region in bright Seyfert galaxies was carried out with the Ohio State CCD spectrograph on the 1.8-m Perkins Telescope at the Lowell Observatory from 1988 to 1997. Data on Akn 120, 3C 120, Mrk 79, Mrk 110, Mrk 335, Mrk 590, and Mrk 817 used here have been published by Peterson et al. (1998a). The data used here on NGC 4051 are preliminary results based on OSU data only, and these are currently being combined with data from other sources.
2. **The International AGN Watch.** Over the last decade, this consortium has carried out multiwavelength monitoring programs on a number of AGNs, and the data are publicly

available<sup>5</sup> (Alloin et al. 1994; Peterson 1999). In this study, we employ the AGN Watch optical data on 3C 390.3 (Dietrich et al. 1998), Fairall 9 (Santos-Lleó et al. 1997), Mrk 509<sup>6</sup> (Carone et al. 1996), NGC 3783 (Stirpe et al. 1994), NGC 5548 (Peterson et al. 1991, 1992, 1994, 1999; Korista et al. 1995), NGC 4151 (Kaspi et al. 1996a), and NGC 7469 (Collier et al. 1998).

3. **The CTIO AGN Monitoring Program.** In connection with the AGN Watch program on NGC 3783 (Stirpe et al. 1994) in 1992, observations of NGC 3227 (Winge et al. 1995) and IC 4329A (Winge et al. 1996) were also made. For the sake of greater internal consistency, we reanalyzed these spectra in the same fashion as the Ohio State monitoring data.
4. **The Wise Observatory QSO Monitoring Program.** A spectroscopic monitoring program on low-redshift quasars is being carried out at the Wise Observatory. Thus far, preliminary results on PG 0804+762 and PG 0953+414 have been published (Kaspi et al. 1996b), and the authors were kind enough to make the original spectra available to us for this analysis.

For each galaxy, we computed the optical continuum– $H\beta$  cross-correlation using the interpolation method of Gaskell & Sparke (1986) as implemented by White & Peterson (1994), and determined the centroid  $\tau_{\text{cent}}$  of the cross-correlation function using all points within 80% of the peak value  $r_{\text{max}}$ . Uncertainties in  $\tau_{\text{cent}}$  were evaluated using the model-independent Monte-Carlo FR/RSS technique of Peterson et al. (1998b). Spectra were combined to form average and root-mean-square (rms) spectra, and the full-width at half maximum of the  $H\beta$  feature in the average and rms spectra was measured, transformed to the rest frame, and is quoted as a Doppler width in kilometers per second.

A summary of the basic data used in this investigation is given in Table 1. The name of the galaxy appears in column (1). Column (2) gives the monochromatic luminosity  $\lambda L_{\lambda}(5100 \text{ \AA})$  (ergs  $\text{s}^{-1}$ ) of the galaxy at a rest wavelength of 5100  $\text{\AA}$ . This is the mean luminosity observed during the monitoring campaign from which the data were drawn. In each case, this has been corrected for Galactic extinction using the  $A_B$  values in the NED database<sup>7</sup>. Columns (3) and (4) give the full-width at half-maximum of the  $H\beta$  emission line in the mean and rms spectra, respectively. Column (5) gives the time lag  $\tau_{\text{cent}}$  for the response of the  $H\beta$  emission line, and the associated uncertainties, which are not symmetric about the measured value.

---

<sup>5</sup>International AGN Watch can be obtained on the World-Wide Web at URL <http://www.astronomy.ohio-state.edu/~agnwatch/>.

<sup>6</sup>Supplemented by additional data from Peterson et al. (1998a).

<sup>7</sup> The NASA/IPAC Extragalactic Database (NED) is operated by the Jet Propulsion Laboratory, California Institute of Technology, under contract with the National Aeronautics and Space Administration.

We expect the line width in the rms spectra to be larger than the line width in the average spectrum because in the former the narrow-line component is eliminated. However there are objects for which the FWHM of lines is *narrower* in the rms spectrum than in the average spectrum. One possible interpretation is that the emission-line gas with the highest velocity dispersion and nearest to the central source, which contributes to the far wings does not vary much, perhaps because it arises in a medium that is optically thin to ionizing radiation (e.g., Shields, Ferland, & Peterson 1995).

Note that for NGC 7469 we give the lag with respect to the UV continuum rather than relative to the continuum at 5100 Å. The reason for this is that in NGC 7469, the optical continuum variations follow those in the ultraviolet continuum by about one day. This is the only AGN in which this effect has been measured (Wanders et al. 1997; Collier et al. 1998; Peterson et al. 1998b).

#### 4. NGC 5548: Evidence for the Keplerian Assumption

The basic assumption of this model is that the line-emitting gas is gravitationally bound, and its velocity dispersion is approximately Keplerian. If this is the case, we would expect that during variations of the ionizing luminosity, the “virial mass”, given by  $M \sim G^{-1}v^2r$  remains constant. While the radius given by the luminosity scaling of the photoionization method (eq. 3) is uncertain, the reverberation radius and the associated velocity derived from the variable part of the line (FWHM-RMS) provide a direct measure of the virial mass.

The virial assumption can be tested for individual objects. It is known that the BLR is stratified, with different emission lines different distances from the central source. Typically different lines also have very different line widths. If the motions in the BLR are dominated by the gravity of the central mass, the Keplerian relation (6) applied to different lines in the same objects must yield the same value for the central mass. Similarly, if the continuum and emission-lines vary over long time scales (the short time scale variability is applied for deriving the reverberation BLR size), the virial mass should remain constant. In other words, above test states that the lags ( $R$ ) of different lines and at different epochs should be anticorrelated with the rms line width as  $R \propto v_{\text{FWHM}}^{-2}$ .

We have tested the virial assumption with the multiyear multiwavelength data on NGC 5548 (Peterson & Wandel 1999). The emission-line lags  $\tau$  range from  $\sim 2$  to  $\sim 30$  days, and are anticorrelated with the line widths  $FWHM$ , consistent with a constant value of the product  $\tau \times (FWHM)^2$ , as expected if the virial assumption is correct. There is significant scatter around the best virial fit to the data, however; we suspect that this is due in part to the fact that both the lag and the line width are dynamic quantities that are changing in response to changes in the continuum flux. Moreover the H $\beta$  results for two years (1993 and 1995) had to be excluded from this analysis because the rms profiles were strongly double peaked and therefore did not yield an

unambiguous line width. Again this suggests to us that while the virial interpretation is correct to first order, it is not the whole story.

Figure 1 shows the virial mass calculated from the reverberation radius and the line width in the rms spectrum as a function of the FWHM-rms for each line in each year. This way of presenting the data enables us to demonstrate that the virial mass of all lines is consistent with a single value.

Fitting an  $M=\text{const.}$  to the points in the  $M$  vs. FWHM plane is equivalent to fitting a line with a slope of -2 ( $\text{lag} \propto (\text{FWHM})^{-2}$ ) in the lag vs. FWHM (log-log) plane (if the two observables were uncorrelated, the best fit would be  $M \propto (\text{FWHM})^2$ ).

We find an average virial mass (weighted by the uncertainties in the mass) of  $(6.1 \pm 2) \times 10^7 M_{\odot}$ . The weighted mean has been calculated as  $\langle x \rangle = \Sigma(x_i/\sigma_i^2)/\Sigma(1/\sigma_i^2)$  where  $\sigma_i$  is the uncertainty in  $x_i$  in the appropriate direction (up or down) with respect to the mean. It is easy to see that all the points in the figure are consistent with the average value within  $\sim 1\sigma$ . While the annual averages of line width and lag in the NGC 5548 data set vary by factors of 2-3 and more than an order of magnitude, respectively, they are anticorrelated in a manner close to the Keplerian relation above, so that the virial mass remains approximately constant (within the uncertainties).

We have calculated the goodness of the  $M=\text{const}$  assumption in three schemes:

- An  $M = \bar{M}$  fit in the  $M$  vs. FWHM plane
- A  $y = -2x + a$  fit in the  $\log(\text{lag})$  vs.  $\log(\text{FWHM})$  plane (that is, x-y plane)
- The best fit  $y = bx + a$  in the  $\log(\text{lag})$  vs.  $\log(\text{FWHM})$  plane

where  $\bar{M}$  is the uncertainty-weighted average reverberation mass,  $x = \log(\text{FWHM})$  and  $y = \log(\tau)$ . We have performed these fits for five data sets:

- All data points
- All lines and  $\text{H}\beta$  represented by the weighted average of the six years ( $\log(\text{FWHM})=3.71$ ,  $\log(\text{lag})=1.25$ )
- All lines from the years 1989 and 1993 (when available), i.e. all lines and  $\text{H}\beta$  from 1989
- Only  $\text{H}\beta$  for the six years, lags from the centroid of the CC function
- Only  $\text{H}\beta$  for the six years, lags from the peak of CC (see below)

The last two sets demonstrate the constancy of the virial mass for time variability of a single line, but evidently the small number of points does not give very significant results. The last set may test the sensitivity of the reverberation scheme to the geometry (see below).

For all sets we have calculated the reduced  $\chi^2$  in the three schemes (table 3) The best fit and the  $\chi^2$  in the (x,y) plane are calculated with weighting by lag uncertainties (Bevington pp. 118 and 188). The errors in the  $x - y$  plane were estimated from the (logarithmic, directional) standard deviation  $\sigma_i$  for each point i,

$$\sigma_i = \log(1 + \sigma_i^+ / \tau_i) \quad \text{if} \quad y_i < bx_i + a_i$$

$$\sigma_i = -\log(1 + \sigma_i^- / \tau_i) \quad \text{if} \quad y_i > bx_i + a_i$$

where  $\sigma_i^+$  and  $\sigma_i^-$  are the + and - uncertainties in the lag  $\tau$ .

Note that the  $M=\text{const}$  fits have lower values of  $\chi^2$  than in the FWHM-lag fits (in the  $x - y$  plane). Although the two are equivalent, the latter uses only the uncertainties in the lag, while the former uses the uncertainties in  $M$ , which combine the lag and FWHM uncertainties, and is therefore more appropriate.

The best fits for the three sets with all lines are consistent with the virial assumption (slope of -2 in the x-y plane). On the other hand, the  $H\beta$  fits are not consistent - this is due to their small dynamical range, which is even reduced by the weighting, as the point with the largest FWHM also has a much larger uncertainty in the lag than the other points. Also the dynamical nature of the lag and line width, which depend on the constantly changing continuum flux is probably contributing to the scatter. Given these factors and the small number of points, this result is probably not very significant. Note however that the  $\chi^2$  tests give a reasonable probability to the  $M=\text{const}$  assumption even for the  $H\beta$  sets, and certainly cannot exclude it.

For the  $H\beta$  annual data we have tried also a different reverberation scheme, using the lags of the peak (rather than the centroid) of the line-continuum CC function. This may give an estimate of how sensitive these results are with respect to the uncertainties of the reverberation technique and its dependence on the BLR geometry (see section 8.2).

The (uncertainty-weighted) mean of the annual virial masses derived from the  $H\beta$  line annual averages is

$$\langle M_{rev-c} \rangle = (6.6 \pm 1.6) \times 10^7 M_\odot \quad H\beta \text{ annual, centroid lag}$$

and

$$\langle M_{rev-p} \rangle = (6.6 \pm 0.5) \times 10^7 M_\odot \quad H\beta \text{ annual, peak lag.}$$

In addition to being mutually consistent, these results are in good agreement with the value derived by using all the available emission-lines and years (altogether 14 data points),

$$\langle M_{rev} \rangle = (6.1 \pm 0.4) \times 10^7 M_\odot \quad \text{different lines, centroid lag.}$$

## 5. The Mass Correlation

The basic procedure is quite straight forward: use rms spectra of the objects with available reverberation analyses, and compare the virial mass calculated this way to the value calculated with the ionization parameter method, using canonical AGN values for  $U n_e$  and  $Q/L$  rather than specific values for each object.

Table 2 compares the BLR sizes and the virial masses derived by the two methods.

We now try to find the correlation and the functional relation between the masses determined by the two methods for the objects with reverberation data. We expect the relation to be linear,  $M_{rev} \propto M_{ph}$ , but we are also testing for a different power-law dependence. Since the parameters that we have approximated appear in the square root, the scatter introduced through these approximation may be small. Since we find that the two mass estimates are well correlated, the correlation may be used to derive a functional dependence — to a first approximation we assume a linear correlation, which gives the normalization coefficient in eq. (4). Figure 2 shows the virial masses calculated by the photoionization (eq. 4) and the reverberation-rms methods.

Considering the unweighted data points gives  $\log(M_{rev}) = 0.82 \log(M_{ph}) + 1.53$  with a correlation coefficient of 0.83.

### 5.1. Weighting by Measurement Uncertainties

Since the uncertainties in  $M_{rev}$  are very different for different objects, it is important to weigh the points according to their uncertainties. Taking into account the directed<sup>8</sup> uncertainties in the  $M_{rev}$  the correlation coefficient becomes 0.89, and the best fit

$$\log(M_{rev}/M_{\odot}) = b \log(M_{ph}/M_{\odot}) + a,$$

with  $b = 0.93 \pm 0.07$  and  $a = 0.70 \pm 0.53$ .

For NGC 5548 masses we have used the weighted averages of the six years. In the weighted fit we have increased the formal uncertainty of the Mrk 590 and NGC 5548 reverberation mass estimates by a factor of  $\sim 3$ , as they were significantly smaller than the other objects, and gave an excessive weight to these points.

---

<sup>8</sup>Directed in the sense of using the appropriate error bar (upper or lower) of each point with respect to the fit, and repeating the fitting until it converged.

## 5.2. Weighting by Intrinsic Uncertainties

We have used the standard procedure of weighting data with uncertainties (Bevington 1969, p. 118) which takes into account only uncertainties in one (the dependent) variable. This weighting method may give too much weight to points with a very small uncertainty in  $M_{rev}$ , since the uncertainty in  $M_{ph}$  is always large, as it has to account for the intrinsic uncertainties in the photoionization method, discussed above. One could apply a “mixed weighting covariance” method, where each data point is weighted considering its  $x$  and  $y$  uncertainties (a detailed discussion of this subject can be found in Feigelson and Babu, 1992). However, also the reverberation method has intrinsic uncertainties, as discussed in section 8 below. The errors quoted for  $M_{rev}$  represent only the formal measurement errors, given by

$$\frac{\Delta M}{M} = \left[ \left( \frac{\sigma_\tau}{\tau} \right)^2 + \left( \frac{2\sigma_V}{V} \right)^2 \right]^{1/2} \quad (7)$$

Therefore also  $M_{rev}$  has an additional intrinsic uncertainty (possibly larger than the measuring errors). Taking into account significant intrinsic uncertainties in both,  $M_{rev}$  and  $M_{ph}$  has the effect of giving all points a similar weight, i.e. an unweighted fit.

## 5.3. Interpreting the $M_{rev} - M_{ph}$ Relationship

Our most important result is the very good correlation, consistent with a linear relation, and the surprisingly low scatter. We note that the outlying objects in our sample are less than a factor of two away from the diagonal ( $M_{ph} = M_{rev}$ ) line.

The slope ( $b$ ) in the logarithmic fit deviating from unity may account for intrinsic residual dependence of the photoionization mass on on parameters such as luminosity or line width, (for example, if one of the parameters in eq. (4), such as  $U$  or  $L_{ion}/L_v$  were dependent on  $L$  or on  $M$ ). The fact that we find the slope to be consistent with unity implies that there is no evidence for such an effect in our sample.

The constant ( $a$ ) in the logarithmic fit gives an estimate of the calibration coefficient, if  $b$  is close to unity. A more direct determination the calibration coefficient is obtained by imposing  $b = 1$  and solving for the best value of  $a$ , which we denote by  $a_1$ . If  $b$  is close to unity, this value is given by

$$\delta_M = \langle y \rangle - \langle x \rangle, \quad (8)$$

where  $\langle x \rangle = \bar{x}$  and  $\langle y \rangle = \bar{y}$  are the averages (weighted, Bevington p. 88, or unweighted, as discussed above). For our sample we find  $\langle \log(M_{rev}/M_\odot) \rangle = 7.49$  and  $7.64$  while  $\langle \log(M_{ph}/M_\odot) \rangle = 7.29$  and  $7.48$ , for the unweighted and weighted averages, respectively, so that  $\delta_M = 0.20$  and  $0.16$ , respectively.

The difference  $\delta_M$  is actually the empirical factor which best calibrates the photoionization method for determining the virial masses, so for the present sample and our choice of parameters we find for the actual coefficient in eq. (4):

$$f = 10^{\delta_M} \approx 1.6 \text{ and } 1.45,$$

respectively.

## 6. The Radius Correlation

The errors in the photoionization virial mass determination (treated in more detail in the discussion section) consist of two main ingredients: the uncertainties introduced by the photoionization method of estimating the BLR size and the uncertainty in matching the size derived to the velocity dispersion implied by the line-width (and which measure of the line profile best describes the relevant velocity dispersion). While these two problems are automatically solved in the reverberation - rms method, it is important to understand their contribution to the errors in the photoionization method.

By comparing the BLR size estimates of the photoionization method with the reverberation radii we can estimate which part of the scatter in the  $M_{ph} - M_{rev}$  correlation (Fig. 2) is due to the uncertainties in the photoionization model approximation and the assumptions of average ionization parameter, density, and  $L_{ion} \approx L_V$ .

The empirical result  $r_{rev} \propto L^{1/2}$  (Kaspi et al. 1997) would predict a linear relation,  $\log(r_{rev}) = 1.0\log(r_{ph}) + C$ , as the photoionization method in its simplest form implies  $r_{ph} \propto L^{1/2}$ .

The data and their interpretation are shown in figures 3a and 3b, respectively: Figure 3a shows the lag vs. the monochromatic luminosity at  $5100\text{\AA}$ . The logarithmic linear (unweighted) fit is  $\log(\text{lag}(\text{days})) = (0.46 \pm 0.1)\log L_{44} + (1.50 \pm 0.11)$  where  $L_{44} = \lambda L_{\lambda}(5100\text{\AA})/10^{44}\text{erg s}^{-1}$ . Within the uncertainties this is consistent with the result of Kaspi et al. (1997). Forcing an  $R \propto L^{1/2}$  slope gives an almost identical result,  $R_{H\beta} = 33L_{44}^{1/2}$  light days, or, expressed in terms of the luminosity integrated over the  $0.1\text{-}1\mu\text{m}$  band rather than the monochromatic luminosity (assuming  $L_{\lambda} \propto \lambda$  or  $F_{\nu} \propto \nu^{-1}$ )

$$R_{H\beta} = 15L_{44,(0.1-1\mu\text{m})}^{1/2} \text{ light days.}$$

Figure 3b shows the lag vs. the BLR size estimated by the photoionization method for our sample. The logarithmic linear fit is  $\log(\text{lag}(\text{days})) = 0.92r(\text{lt-days}) + 0.45$ . The correlation ( $r = 0.70$ ) is significantly less good than the correlation of the masses. This is caused by a few objects with large uncertainties being well off the diagonal. When the points are weighted by the lag uncertainties, the slope becomes more deviant from unity —  $b = 1.3 \pm 0.12$  — because several off-diagonal objects with small uncertainties dominate the fit. As discussed above, the unweighted fit may be more realistic as it approximately gives the result of adding the intrinsic uncertainties.

Effectively it softens the influence of the objects with very small lag error bars in the weighting, lowering the slope back to be consistent with unity.

It is interesting to determine the calibration coefficient also for the BLR size, derived from the photoionization method. Considering figure 3b, the weighted averages are  $\langle \log(\text{lag}) \rangle = 1.22$  and  $1.31$  and  $\langle \log(r_{ph}) \rangle = 0.81$  and  $0.94$  for the unweighted and weighted methods, respectively. The calibration factor  $\delta_R = \langle \log(\text{lag}) \rangle - \langle \log(r_{ph}) \rangle$  is then  $0.39$  and  $0.37$ , so that the radius calibration factor is

$$f_R \approx 10^{\delta_R} = 2.4 \quad (9)$$

for both weighting methods. We see that the correlation between the BLR sizes given by the reverberation and photoionization methods is significantly weaker than the corresponding correlation between the masses and the scatter is larger.

## 7. Estimating $L_{ion}$ and $L/M$

### 7.1. The Ionizing Luminosity

The coefficient in eq. (4) is  $f = \frac{3}{4} f_L^{1/2} \bar{E}_1^{-1/2}$ . We may reverse this equation and use the value we have found for  $f$  in order to calculate the effective ratio  $f_L$  between the visual luminosity  $\lambda L_\lambda(5100 \text{ \AA})$  and the ionizing luminosity:

$$f_L = \left( \frac{4}{3} f \right)^2 \bar{E}_1 \approx 1.8 \times 10^{2\delta_M} \bar{E}_1 \approx 4\bar{E}_1,$$

However, the empirical factor  $f$  actually accounts for two components: the luminosity factor,  $f_L$ , and the kinematic factor,  $f_k$ , which we have taken to be  $\frac{3}{4}$  in both methods, but it may contain also a possible factor contributed by the mapping from the FWHM in the photoionization method to the FWHM-RMS in the reverberation method.

A more direct determination of  $f_L$  can be obtained from the calibration factor of the BLR sizes: since  $R_{ph} \propto L_{obs}^{1/2}$  while the true emission-line radius measured by the lag is  $R_{rev} \propto L_{ion}^{1/2}$ , we have  $L_{ion}/L_{obs} \propto (R_{rev}/R_{ph})^2$ . In our notation, eq. (3) gives

$$f_L = U n_{10} \bar{E}_1 \left( \frac{\langle R_{rev} \rangle}{\langle R_{ph} \rangle} \right)^2 \quad (10)$$

which for our choice,  $U n_{10} = 1$  becomes

$$f_L = 10^{2\delta_R} \bar{E}_1 = 6\bar{E}_1$$

. For reasonable ionizing spectra (Wandel 1997, Bechtold et al. 1987)  $\bar{E} \sim 1.2 - 2$ , so that that for our sample the ionizing continuum may be related to the monochromatic luminosity at  $5100 \text{ \AA}$  by

$$L_{ion} \approx 10 U n_{7-12} \lambda L_\lambda(5100 \text{ \AA}).$$

For example, we can compare this empirical estimate of the average photon energy to some published model estimates. Integrating the "Medium" AGN spectrum described in Bechtold et al. (1987) gives a total bolometric luminosity of 1.4 times the value of  $\nu L_\nu$  at 1 Rydberg, which equals 7.7 times the value of  $\nu L_\nu$  at 5100 Å. The exact values are relatively insensitive to the upper limit to the energy integral (the choice of hard-X-ray cutoff). About half of this total power is emitted by the "power-law" component longward of 1500 Å. For Bechtold et al.'s "Hard" AGN continuum energy distribution, a somewhat smaller fraction of the total bolometric power emerges at wavelengths longer than 1 Ryd, and the total bolometric power is 13 times the value of  $\nu L_\nu$  at 5100 Å. Within the uncertainties on average BLR parameters, either of these models is consistent with the average AGN continuum spectrum inferred from our comparison of photoionization and reverberation estimates of BLR size.

## 7.2. The Eddington Ratio

We may use the high quality virial mass estimates obtained by the reverberation -RMS method for this sample, to estimate a mean  $L/M$  relation. Combining this with the above estimate of the ionizing luminosity (which presumably is comparable to the total bolometric luminosity, as a large part of the AGN energy is expected to be radiated in the UV) we may estimate the Eddington ratio.

Figure 4 shows the reverberation - RMS virial mass vs. the 5100 Å luminosity for our sample.

An unweighted linear fit gives  $\log(M/M_\odot) = 0.54 \log(L_{44}) + 7.94$ , with a correlation coefficient  $r = 0.68$ . However, here the fit needs to be weighted only by the mass uncertainties, as those of the luminosity are relatively small. A weighted fit yields

$$\log(M/M_\odot) = (0.77 \pm 0.07)\log(L_{44}) + (7.92 \pm 0.04). \quad (11)$$

We can calculate the Eddington ratio from the difference of the weighted averages,

$$\delta_{ML} = \langle \log(M/M_\odot) \rangle - \langle \log(L_{44}) \rangle = 8.0. \quad (12)$$

Combining this with the definition of the Eddington luminosity  $L_{Edd} = 1.3 \times 10^{38} (M/M_\odot) \text{ erg s}^{-1}$  we have for our sample

$$\lambda L_\lambda(5100 \text{ Å}) \approx 0.01 L_{Edd} \quad (13)$$

and

$$L_{ion}/L_{Edd} \approx 0.1 U n_{10}. \quad (14)$$

### 7.3. Ionizing luminosities of individual objects

We may apply eq. 10, (or inverse eq. (3)) to estimate the ionizing luminosity of individual objects in our sample. This gives

$$L_{ion} \approx \bar{E}_1 U n_{10} \lambda L_\lambda(5100 \text{ \AA}) \left( \frac{R_{rev}}{R_{ph}} \right)^2 = 6 \times 10^{43} E_1 U n_{10} \left( \frac{\tau}{10 \text{ days}} \right)^2 \text{ erg s}^{-1}, \quad (15)$$

where  $\tau$  is the lag (the centroid of the cross-correlation function). Since the ionizing luminosity is likely to be a large fraction of the bolometric luminosity, and the virial reverberation -rms mass is our most reliable estimate of the mass of the central black hole, these values give a direct measure of the true Eddington ratio

$$L/L_{Edd} \approx L_{ion}/M_{rev}.$$

The last two columns in table 2 show the ionizing luminosity and total Eddington ratio of the objects in our sample.

Fig. 5 shows the virial (reverberation) mass vs. the ionizing luminosity for the objects in our sample. We note that most objects in our sample have  $L/L_{Edd} \sim 0.01 - 0.3$ . We also note that there is a strong trend of the Eddington ratio to increase with luminosity: an unweighted fit to the Eddington ratio vs. luminosity gives

$$L/L_{Edd} = 0.08 L_{44}^{0.7},$$

where  $L_{44}$  is the luminosity at 5100Å. However, since  $L_{ion} \propto \tau^2$  (eq. 15) and  $M \propto \tau \times (FWHM)^2$ , this correlation may be a mere reflection of the correlation of the lag with luminosity.

## 8. Discussion

### 8.1. Results

From the present sample we find that the virial masses of the 19 AGN in our sample estimated by the photoionization method are very well correlated with the more direct estimates from the reverberation - RMS method. We find the relation is consistent with a linear one, that is,  $M_{rev} \propto M_{ph}$ . For an average value of  $U n_e = 10^{10}$  and assuming  $L_{ion} = f_L \lambda F_\lambda(5100 \text{ \AA})$  we find a calibration factor of  $f \approx 1.5$  where  $M_{rev} = f M_{ph}$ , which corresponds to  $f_L \approx 10$ .

The fact that the photoionization masses are better correlated with the reverberation - RMS masses than the corresponding BLR size with the reverberation distances contradicts the intuitive prediction that the scatter in the masses should be larger, due to the additional uncertainty in translating line profiles to the appropriate velocity dispersion. This may indicate that there is an internal compensation mechanism, which reduces scatter in the photoionization mass determination. This may be related to the difference between the reverberation and the

photoionization methods: the former measures the size of the variable component of the BLR, while the latter measures the emissivity-weighted size, and the two may differ. However, when applied to the virial mass, both methods measure the same mass.

This conclusion is strongly supported by the variability of NGC 5548 (Fig. 1), where the variations in the lag of the line width are significantly larger than the variations in the combination  $\text{lag} \times v_{\text{FWHM}}^2$ . (The latter is actually consistent with remaining constant, within the uncertainties).

Also, examining the deviations of individual objects from the linear relation in the mass and size plots, we note that several objects which deviate significantly in Fig. 4 (the BLR size correlation) have smaller deviations in the mass correlation (Fig. 3).

We have also estimated the ionizing luminosity, the mass-luminosity relation and the Eddington ratio for our sample. Applying the calibrated photoionization method to many AGN may reveal a trend for these important parameters in various groups of AGN.

Obtaining reliable black hole masses for many AGN may also provide important insight for the relation between AGNs and their host galaxies, as has already been demonstrated for the present sample (Wandel 1999).

## 8.2. Comparison with Accretion-Disk Models

AGN masses may be estimated also by fitting the continuum optical-UV spectrum by a thin accretion disk model spectrum (e.g. Malkan 1990; Wandel and Petrosian 1988; Laor 1990). We have compared the reverberation and photoionization mass estimates with those obtained by standard thin-accretion disk fitting of the continuum energy distribution. Specifically, more than half of the calibrating Seyfert 1's have been fitted in Sun and Malkan (1989), Malkan (1990), and Alloin et al. (1995). The black hole masses estimated from continuum fitting are generally correlated with those derived from the emission lines. We find that in general the black hole mass obtained from the accretion disk method tends to be larger than the mass found from the reverberation data. In order for the normalizations to be consistent with the reverberation masses the parameters of the disk models have to be chosen to give the smallest possible black hole masses. Specifically, the disk fits must all assume non-rotating (Schwarzschild) black holes, and zero inclination (face on) to give a normalization consistent with the emission line estimates. For most of the objects in our sample, inclined disks, or rotating (Kerr) black holes would yield larger continuum-fitting black hole masses, inconsistent with the emission line fits. While for Kerr black hole accretion disk models the black hole mass required to fit a given continuum depends sensitively on the inclination, the dependence in the Schwarzschild case is much less steep. For a Schwarzschild black hole one may therefore soften the constraint of small inclination, taking into account the intrinsic uncertainties in the mass determination and in the accretion disk fitting method. This argument and the constraint of low black hole masses seem to infer that black holes in AGN (at least in the Seyfert 1 galaxies in our sample) tend to have

little or no rotation, being near-Schwarzschild . This subject will be elaborated in a separate work.

### 8.3. Selection effects

A major question that comes up when trying to apply the calibration result obtained from this sample to other AGNs without is whether the sample is representative. The objects in our sample - AGNs with adequate reverberation data - were selected by the criteria that make them "promising" for reverberation mapping: evidence or good chances to observe continuum and emission-line variability. In most cases this meant some previous indication that the emission-lines varied. The evident selection criterion is therefore variability, in particular emission-line variability. However, variability is a feature common to many if not most AGNs, and it is difficult to identify an obvious way how such selection criteria can bias our results. If, for example, the more variable sources had systematically broader mean  $H\beta$  line profiles, then the black hole masses derived using the coefficient from our sample would be underestimated.

However, the line width enters in the same way in both mass estimation methods, only it is the mean profile in the photoionization method and the rms profile in the reverberation one, so it is the difference between the mean and rms profile width which should be considered, and that one shows no trend with luminosity (Fig. 6). We also note that the FWHM difference shows no preferred direction: it is positive for some objects and negative for others.

Another question that may be posed is whether the selection on objects on the basis of emission-line-variability introduces a bias at the parameter-space coverage: whether our sample is representative of the AGN population. We have plotted our sample together with large samples of PG quasars and Seyfert 1 galaxies (both, narrow and broad line Seyferts) in the luminosity vs.  $H\beta$  line-width plane (Fig. 7). We can see that our sample provides a fair representation of the local AGN population, except of the high luminosity end. This limitation can be expected, as the BLR size is correlated with luminosity, so very luminous objects are likely to have larger BLRs, and hence longer response times, hence they would be more difficult for reverberation measurement. However, as Fig. 7 reveals no obvious correlation between luminosity and line width, this restriction is not likely to bias our results.

### 8.4. Uncertainties of the reverberation method

Although the BLR sizes determined from the lag are much more reliable than those given by the photoionization method, which involves much larger intrinsic uncertainties (see below), it has uncertain factors depending on the geometry of the emitting gas:

- What is the error introduced by using moments of the transfer function rather than the full function? The shape of the cross-correlation function depends not only on the transfer

function, but also on the form of the continuum variations, so one can't read much from it. However, its first moment (the centroid) is rather less dependent on the form of the continuum variations. To REALLY address the problem correctly, one needs the transfer functions, but accurate transfer recovery is somewhat beyond the scope of what can be done with the data we have at present.

- How is the lag time related to the geometrical distance of the line emitting gas from the illuminating continuum, and how does it depend on the geometry, in particular of a radially extended distribution? Also here there is a dependence on the continuum variations. For example, if the emitting region has an extended range of radii,  $R_{in} - R_{out}$  the outer parts will not be able to respond to continuum changes with a timescale shorter than  $\sim R_{out}/c$ , while the inner parts will. In that case a more adequate measure of the size may be obtained using the peak rather than the centroid of the cross-correlation function.

More uncertainties are introduced by combining the lag with the line profile to give a mass estimate:

- What measure of the line profile gives the appropriate velocity dispersion to combine with the lag? This becomes more complicated when the line emitting gas has a radially extended geometry, as the centroid lag, which is the responsivity weighted delay, may be differently weighted than the FWHM, which is the emissivity weighted line-of-sight velocity dispersion.
- Does the width of line profile measure the velocity dispersion in the same gas the distance of which is measured by the lag? Using the rms rather than the mean profile reduces, but does not eliminate this uncertainty.
- What is the relationship between the emissivity-weighted line-of-sight velocity measured by the line width and the central mass? This would depend on the shape of the orbits, which may introduce a systematic variation of a factor of a few.
- What happens if the illuminating radiation does not originate directly from the central mass? In that case the lag and the line width would refer to different parts, the combination of which to give a virial mass estimate would depend on the specific geometry.

All the above uncertainties are systematic, and introduce an error factor of a few, significantly larger than the random errors quoted in table 1. However, being systematic uncertainties, they will apply to all objects alike, altering the calibration coefficient but not effecting the linear correlation between the masses derived by the two methods. However, if there were luminosity-dependent effects, for example if the BLR geometry would change with  $L$ , or if the relation between the rms and the mean line width depended on  $L$  - or on  $M$  - this would change the slope of the correlation. As seen from Fig 6, such a systematic difference between the rms and mean FWHM in our sample is not present.

### 8.5. Uncertainties of the photoionization method

The basic photoionization method applied above to check the feasibility of the calibration makes several simplifying assumptions, which need to be examined in more detail or replaced by a more elaborate treatment.

- Potential ambiguities arise as a result of the radial extent and ionization stratification of the BLR. The effect of these complications may be studied within the framework of the locally maximally emitting cloud model (Baldwin et al. 1995; Korista et al. 1995).
- The physical parameters used to calculate the distance (density and ionization parameter) may vary from object to object and differ also for different lines in the same object. The adjustable factor in the basic photoionization method depends on the values used for the “average” ionization parameter, density, and  $L/L_{ion}$ . It is possible to use spectral data on different emission lines, to estimate the values of the ionization parameter and density for individual objects.
- The mapping from the line width to the actual virial velocity depends on the distribution of the line emission in physical and velocity space, and how this is related to the line-width measure (e.g., FWHM, FWZI, intermediate width, skewness). The convolution of extended-emission BLR models with various possible dynamics of the BLR gas may be used to find an improved relation between the line profile and the effective velocity dispersion in the line emitting gas, induced by the central mass.
- In extended BLR geometries, also the physical characteristics (such as density, differential covering area, emissivity) are likely to vary with radius, as indicated e.g. by two-zone photoionization modeling of several line ratios, which suggests a stratified BLR possibly extending into an “intermediate line region” (Brotherton et al. 1994).

Compensating for these potential ambiguities in the photoionization method may give an improved photoionization method of virial mass determination, and may also reduce the systematic error sources in the photoionization mass estimates and the scatter in the  $M_{ph}$  vs.  $M_{rev}$  diagram.

Comparing masses and BLR sizes obtained by improved photoionization models to the reverberation - RMS values may in turn be used to test the photoionization BLR models.

## 9. Summary

We have estimated the virial mass of 19 AGN from the BLR size and emission-line width, using two different methods: the accurate reverberation mapping combined with the variable part of the emission-line, and the photoionization method, combined with the plain line width. We have shown that the two mass estimates for all objects in our sample are highly correlated, and

consistent with a linear relation, hence we were able to calibrate the photoionization method of mass and BLR size estimate. This should make possible mass estimates for virtually all AGN with  $H\beta$  line width measurements, which will be presented in a subsequent work. Our sample significantly enhances the available AGN central mass estimates: it has twice the number of objects previously available, it has better mass values, using the rms rather than the mean line profile, and all objects are uniformly treated. The calibration also enables us to estimate the ionizing luminosity, which cannot be directly observed. For our sample we find it to be on average 10 times the monochromatic luminosity at  $5100\text{\AA}$ . Combining the ionizing luminosities with the reverberation mass estimates our sample gives a mass-luminosity relation of  $M \propto L^{0.8}$ , with an Eddington ratio distributed in the range 0.01–0.3.

We are grateful to Shai Kaspi and Hagai Netzer, for permission to use the Wise Observatory data prior to publication, and to the anonymous referee for valuable suggestions. AW acknowledges the hospitality of the Astronomy Department at UCLA. We are grateful for support of this work by the National Science Foundation through grant AST–9420080 to The Ohio State University.

## REFERENCES

- Alloin, D. et al. 1995 *A& A*, 293, 293.
- Alloin, D., Clavel, J., Peterson, B.M., Reichert, G.A., & Stirpe, G.M. 1994, in *Frontiers of Space and Ground-Based Astronomy*, ed. W. Wamsteker, M.S. Longair, & Y. Kondo (Dordrecht: Kluwer), p. 423
- Baldwin, J.A. et al. 1995, *ApJ*, 455, L118
- Bechtold, J., Weymann, R.J., Lin, Z., Malkan, M.A. 1987, *ApJ*, 315, 180
- Bevington, P.R. 1969, *Data Reduction and Error Analysis for the Physical Sciences*, McGraw–Hill
- Blandford, R.D. & McKee, C.F. 1982, *ApJ*, 255, 419
- Boller, Th., Brandt, N. and Fink, V. 1996, *A& A* 305, 53
- Boroson, T. and Green, R.F. 1992, *ApJS* 80, 109
- Brotherton, M.S. et al. 1994, *ApJ*, 430, 495
- Carone, T.E., et al. 1996, *ApJ*, 471, 737
- Collier, S., et al. 1998, *ApJ*, 500, 162
- Dietrich, M., et al. 1998, *ApJS*, 115, 185
- Feigelson, E.D. and Babu, G.J. 1992, *ApJ* 397, 55.
- Gaskell, C.M., & Sparke, L.S. 1986, *ApJ*, 305, 175
- Gaskell, C.M. 1988, *ApJ*, 325, 114

- Joly, M., Collin-Souffrin, S., Masnou, J.L., & Nottale, L. 1985, *A&A*, 152, 282
- Kaspi, S., et al. 1996a, *ApJ*, 470, 336
- Kaspi, S., Smith, P.S., Maoz, D., Netzer, H., & Jannuzi, B.T. 1996b, *ApJ*, 471, L75
- Kaspi, S. 1997, in *Emission Lines in Active Galaxies: New Methods and Techniques*, ed. B.M. Peterson, F.-Z. Cheng, and A.S. Wilson, (San Francisco: ASP), p. 159
- Koratkar, A.P., & Gaskell, C.M. 1991, *ApJS*, 75, 719
- Korista, K.T., et al. 1995, *ApJS*, 97, 285
- McIntosh, D.H., Rieke, M.J., Rix, H.-W., Foltz, C.B., & Weymann, R.J., 1999, *ApJ*, in press (astro-ph/9810287).
- Laor, A. 1990, *MNRAS* 246, 369 Laor, A., Fiore, F., Elvis, M., & Wilkes, B., 1998 *ApJ*,
- Krolik, J.H., Horne, K., Kallman, T.R., Malkan, M.A., Edelson, R.A., & Kriss, G.A. 1991, *ApJ*, 371, 541
- Malkan, M.A. 1990, in *IAU Colloquium no. 129, "Structure and Emission Properties of Accretion Disks"*, eds. C. Bertout et.al., Editions Frontiers: Paris, p. 165.
- Mathews, W.G., & Ferland, G.J. 1989, *ApJ*, 323, 456
- Murray, N. 1998, *ApJ* 494, 125 Netzer, H. 1990 in *Active Galactic Nuclei, Saas-Fee Advanced Course 20*, eds. T.J.-L. Courvoisier and M. Major, (Berlin: Springer-Verlag), p. 57
- Netzer, H., & Peterson, B.M. 1997, in *Astronomical Time Series*, ed. D. Maoz, A. Sternberg, and E.M. Leibowitz, (Dordrecht: Kluwer), p. 85
- Penston, M.V. 1991, in *Variability of Galactic Nuclei*, ed. H.R. Miller & P.J. Wiita (Cambridge Univ. Press), p.343.
- Peterson, B.M. 1999, in *Structure and Kinematics of Quasar Broad Line Regions*, ed. C.M. Gaskell, W.N. Brandt, D. Dultzin-Hacyan, M. Dietrich, and M. Eracleous (San Francisco: ASP), in press
- Peterson, B.M., et al. 1991, *ApJ*, 368, 119
- Peterson, B.M., et al. 1992, *ApJ*, 392, 470
- Peterson, B.M., et al. 1994, *ApJ*, 425, 622
- Peterson, B.M. & Wandel, A. 1999, *Ap.J.Lett*, submitted
- Peterson, B.M., Wanders, I., Bertram, R., Hunley, J.F., Pogge, R.W., & Wagner, R.M. 1998a, *ApJ*, 501, 82
- Peterson, B.M., Wanders, I., Horne, K., Collier, S., Alexander, T., & Kaspi, S. 1998b, *PASP*, 110, 660
- Peterson, B.M. et al. 1999, *ApJ*, 510, 659.
- Rees, M., Netzer H., & Ferland, G.J. 1989 *ApJ*, 347, 640

- Rokaki, E., Collin-Souffrin, S., & Magnan, C. 1993, *A&A*, 272, 8
- Rokaki, E., Boisson, C., & Coullin-Suffrin, S. 1992, *A&A*, 253, 57
- Rosenblatt, E., Malkan, M., Sargent, W., & Readhead, A. 1994, *ApJS*, 93, 73
- Santos-Lleó, M., et al. 1997, *ApJS*, 112, 271
- Shields, J.C., Ferland, G.J., & Peterson, B.M. 1995, *ApJ*, 441, 507
- Stirpe, G.M., et al. 1994, *ApJ*, 425, 622
- Sun, W-H, and Malkan, M.A. 1989, *ApJ* 346, 68
- Wandel, A. 1997, *ApJ*, 430, 131.
- Wandel, A. 1998, in *Structure and Kinematics of Quasar Broad Line Regions*, ed. C.M. Gaskell, W.N. Brandt, D. Dultzin-Hacyan, M. Dietrich, and M. Eracleous (San Francisco: ASP), in press (astro-ph 9808171).
- Wandel, A. 1999, *ApJL*, in press.
- Wandel, A. & Boller, Th. 1998, *A&A*, 331, 884
- Wandel, A. & Mushotzky, R.F. 1986, *ApJ*, 306, L61
- Wandel, A. and Petrosian, V. 1988, *ApJL* 329, 11.
- Wandel, A., & Yahil, A. 1985, *ApJ*, 295, L1
- White, R.J., & Peterson, B.M. 1994, *PASP*, 106, 879
- Winge, C., Peterson, B.M., Horne, K., Pogge, R.W., Pastoriza, M.G., & Storchi-Bergmann, T., 1995, *ApJ*, 445, 680
- Winge, C., Peterson, B.M., Pastoriza, M.G., & Storchi-Bergmann, T., 1996, *ApJ*, 469, 648
- Zheng, W., Kriss, G.A., Telfer, R.C., Grimes, J.P., & Davidsen, A.F. 1997, *ApJ*, 475, 469

Fig. 1.— The virial mass of NGC 5548 vs. FWHM-rms for  $H\beta$  (6 observing seasons in the years 1989-1996) and five other lines in the years 1989 and 1993 (see text). Data taken from table 1 of Peterson and Wandel (1999).

Fig. 2.— Virial mass obtained from the reverberation-rms data vs. the virial mass estimated by the photoionization method. The dotted line shows the best linear ( $M_{rev} \propto M_{ph}$ ) fit weighted by the uncertainty in  $M_{rev}$  for each object.

Fig. 3.— a. Reverberation centroid lags vs monochromatic luminosity at  $5100\text{\AA}$ . b. Reverberation radius vs. BLR size estimated with the photoionization method. The dotted line shows the best linear ( $\tau \propto L^{1/2}$  or  $R_{rev} \propto R_{ph}$ ) fit weighted by the uncertainties in the lag. Formally, the uncertainties in the photoionization estimates are the uncertainties in  $L(5100\text{\AA})$  which are very small. The intrinsic uncertainties in the photoionization estimates are not shown.

Fig. 4.— Reverberation-RMS mass vs. monochromatic luminosity. The dotted line shows the best linear ( $M_{rev} \propto L$ ) fit weighted by the uncertainties in  $M_{rev}$ .

Fig. 5.— Ionizing luminosity (derived from the lag, see text) vs. reverberation-RMS mass. The diagonal lines correspond to an Eddington ratio of 1 and 0.01.

Fig. 6.— The fractional difference between the rms and mean FWHM( $H\beta$ ) line profiles (FWHM difference divided by FWHM(rms)) vs. luminosity.

Fig. 7.— The reverberation AGN sample (circles) in the visual luminosity vs. FWHM( $H\beta$ ) plane compared to other AGN: PG quasars (diamonds; from Boroson and Green, 1994) and Seyfert 1 galaxies (triangles; from Boller, Brandt and Fink, 1996). Open circles indicate the six years of data for NGC 5548.

Table 1: Continuum Luminosity, FWHM H $\beta$  (mean and rms), and Continuum-Line Lags

Name	$\log \lambda L_{\lambda}(5100\text{\AA})$ (erg s $^{-1}$ )	$v_{\text{FWHM}}(\text{mean})$ (km s $^{-1}$ )	$v_{\text{FWHM}}(\text{rms})$ (km s $^{-1}$ )	lag $\tau_{\text{cent}}$ (days)
3C 120	43.59	1910	2210 $\pm$ 120	43.8 $^{+27.7}_{-20.3}$
3C 390.3	43.53	10000	10500 $\pm$ 800	24.2 $^{+6.7}_{-8.4}$
Akn 120	43.89	5800	5850 $\pm$ 480	38.6 $^{+5.3}_{-6.5}$
F 9	44.01	5780	5900 $\pm$ 650	17.1 $^{+3.5}_{-8.0}$
IC 4329A	42.86	5050	5960 $\pm$ 2070	1.4 $^{+3.4}_{-2.9}$
Mrk 79	43.36	4470	6280 $\pm$ 850	18.1 $^{+4.9}_{-8.6}$
Mrk 110	43.31	1430	1670 $\pm$ 120	19.5 $^{+6.5}_{-6.8}$
Mrk 335	43.53	1620	1260 $\pm$ 120	16.8 $^{+5.2}_{-3.3}$
Mrk 509	43.91	2270	2860 $\pm$ 120	79.3 $^{+6.5}_{-6.2}$
Mrk 590	43.44	2470	2170 $\pm$ 120	20.5 $^{+4.5}_{-3.0}$
Mrk 817	43.46	4490	4010 $\pm$ 180	15.5 $^{+4.3}_{-3.5}$
NGC 3227	42.07	4920	5530 $\pm$ 490	10.9 $^{+5.6}_{-10.9}$
NGC 3783	42.79	3790	4100 $\pm$ 1160	4.5 $^{+3.6}_{-3.1}$
NGC 4051	41.47	1170	1230 $\pm$ 60	6.5 $^{+6.6}_{-4.1}$
NGC 4151	42.62	5910	5230 $\pm$ 920	3.0 $^{+1.8}_{-1.4}$
NGC 5548 <sup>a</sup>	43.21	6300	5500 $\pm$ 400	21.6 $^{+2.4}_{-0.7}$
NGC 7469 <sup>b</sup>	43.54	3000	3220 $\pm$ 1580	5.0 $^{+0.6}_{-1.1}$
PG 0804+762	44.52	3090	3870 $\pm$ 110	100.0 $^{+16.3}_{-19.8}$
PG 0953+414	44.82	2890	3140 $\pm$ 350	107.1 $^{+71.2}_{-58.0}$

<sup>a</sup>For NGC 5548, the lag and the FWHM(rms) are derived from the whole data set of the years 1989–1996.

<sup>b</sup>For NGC 7469, the cross-correlation lags are relative to the ultraviolet continuum variations at 1315 Å on account of the wavelength-dependent continuum time delays (see Wanders et al. 1997; Collier et al. 1998; Peterson et al. 1998b).

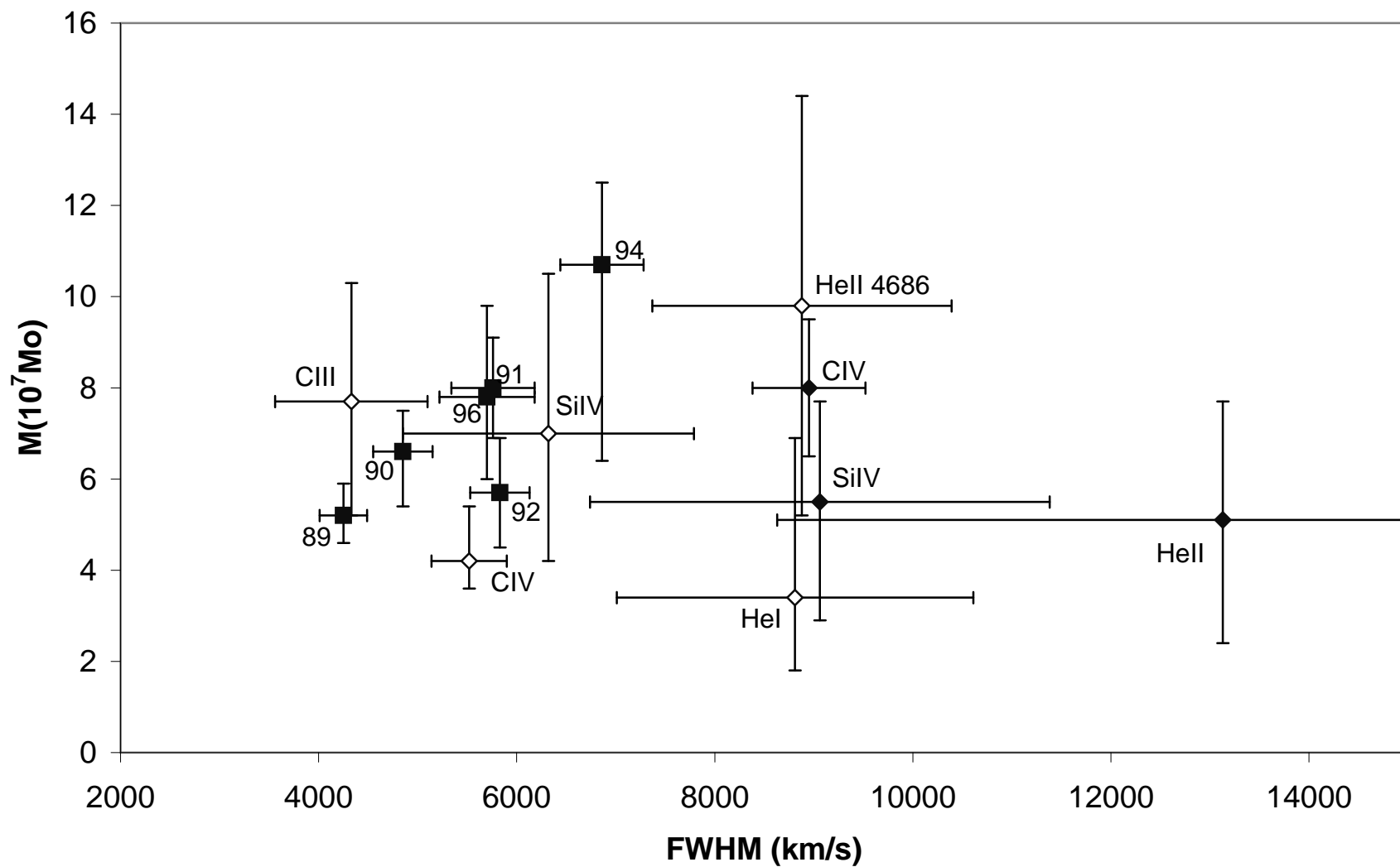
Table 2: Reverberation BLR Sizes and Central Masses, Compared with Photoionization Sizes and Masses. The last two columns give the ionizing luminosity (derived from the lag, see text) and the corresponding Eddington ratio

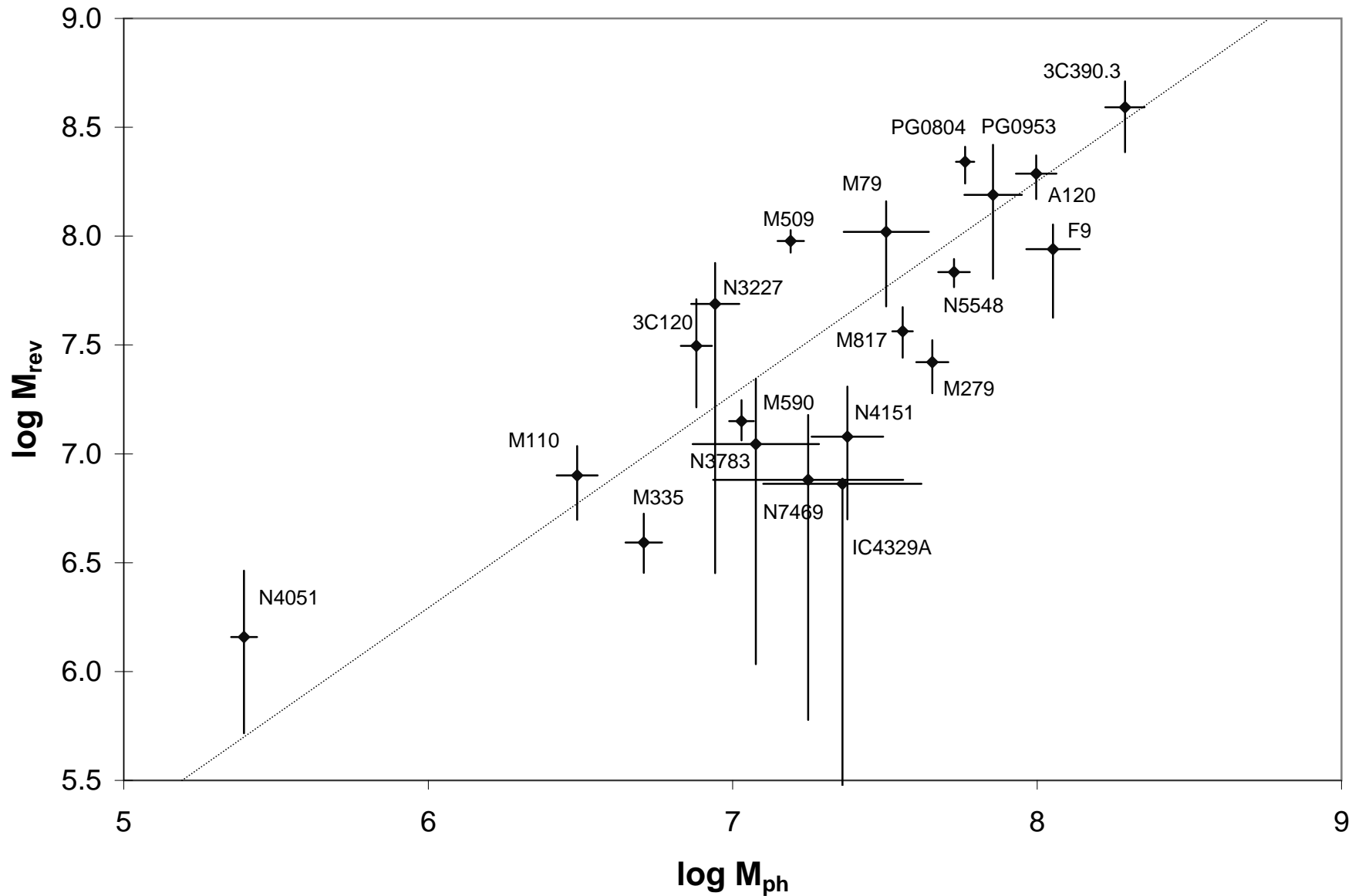
Name	$\log R_{ph}$	$\log \text{lag}$	$\log M_{ph}$	$\log M_{rev}$	$M_{rev}(10^7 M_{\odot})$	$\log L_{ion}$	$\log(L_{ion}/L_{Edd})$
3C 120	0.92	1.64	6.86	7.49	$3.1^{+2.0}_{-1.5}$	45.03	-0.57
3C 390.3	0.89	1.38	8.26	8.59	$39.1^{+12}_{-15}$	44.51	-2.19
Akn 120	1.07	1.59	7.97	8.29	$19.3^{+4.1}_{-4.6}$	44.92	-1.48
F 9	1.13	1.23	8.03	7.94	$8.7^{+2.6}_{-4.5}$	44.21	-1.84
IC 4329A	< 0.56	0.15	7.34	< 6.86	< 0.73	< 42.04	< -2.93
Mrk 79	0.81	1.26	7.48	8.02	$10.5^{+4.0}_{-5.7}$	44.26	-1.87
Mrk 110	0.78	1.29	6.46	6.91	$0.80^{+0.29}_{-0.30}$	44.33	-0.69
Mrk 335	0.89	1.23	6.68	6.58	$0.39^{+0.14}_{-0.11}$	44.20	-0.49
Mrk 509	1.08	1.90	7.17	7.98	$9.5^{+1.1}_{-1.1}$	45.54	-0.54
Mrk 590	0.85	1.31	7.00	7.15	$1.4^{+0.3}_{-0.3}$	44.37	-0.89
Mrk 817	0.86	1.19	7.53	7.56	$3.7^{+1.1}_{-0.9}$	44.13	-1.54
NGC 3227	0.16	1.04	6.92	7.69	$4.9^{+2.7}_{-5.0}$	43.82	-1.98
NGC 3783	0.52	0.65	7.05	7.04	$1.1^{+1.1}_{-1.0}$	43.05	-2.10
NGC 4051	-0.14	0.81	5.37	6.15	$0.14^{+0.15}_{-0.09}$	41.57	-0.84
NGC 4151	0.44	0.48	7.35	7.08	$1.2^{+0.8}_{-0.7}$	42.70	-2.49
NGC 5548	0.73	1.26	7.70	7.83	$6.8^{+1.5}_{-1.0}$	44.27	-1.83
NGC 7469	0.90	0.70	6.87	6.88	$0.76^{+0.75}_{-0.76}$	43.14	-1.86
PG 0804+762	1.39	2.00	7.74	8.34	$21.9^{+3.8}_{-4.5}$	45.75	-0.70
PG 0953+414	1.54	2.03	7.83	8.19	$15.5^{+10.8}_{-9.1}$	45.81	-0.49

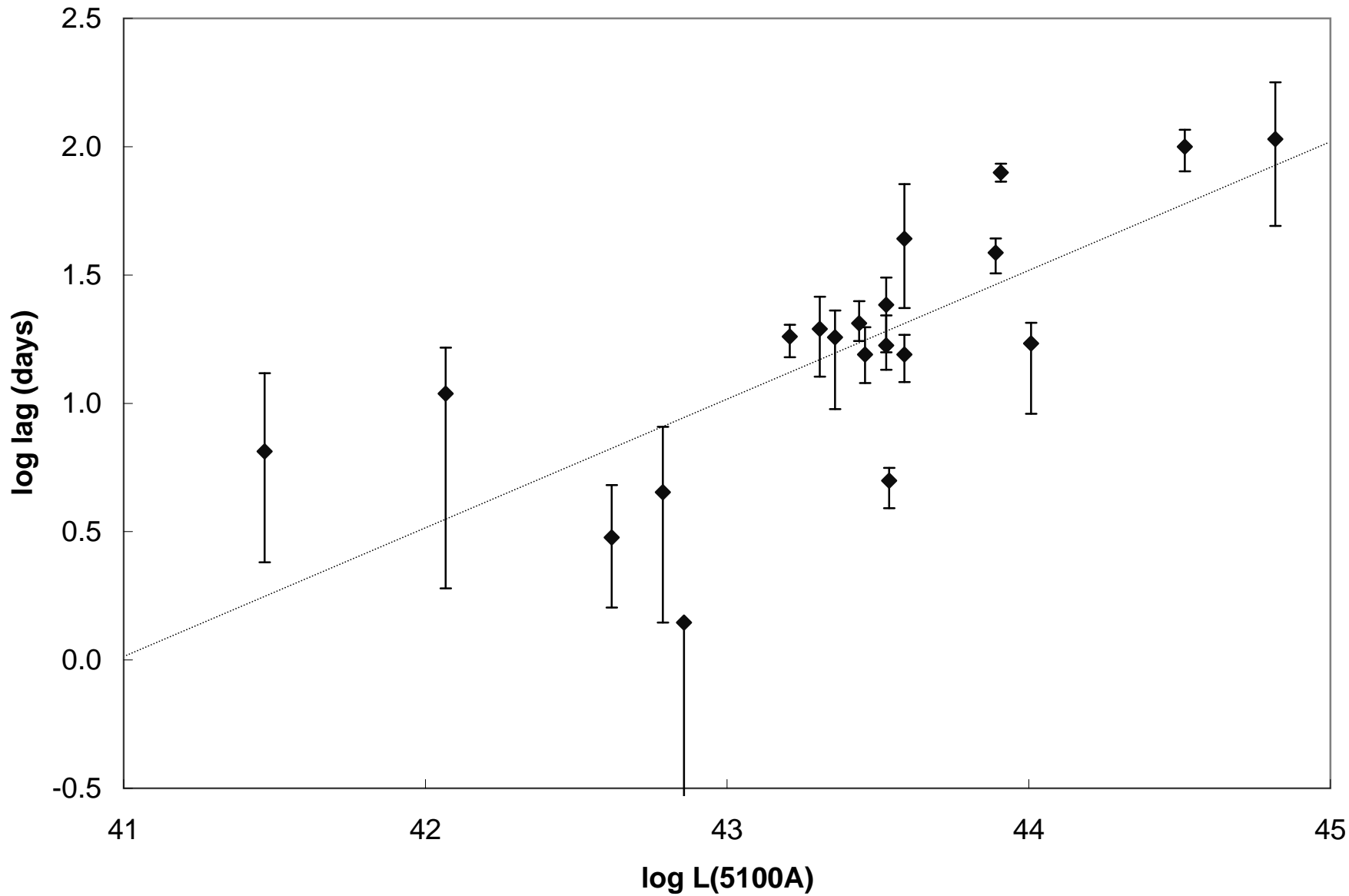
Table 3: Reduced  $\chi^2$  and probabilities (in parenthesis) for the three fitting schemes, constant mass (columns 3-4),  $\text{lag}\propto (FWHM)^2$  ( $y=-2x+a$ , columns 5-6), and the best fit ( $y=-bx+a$ , columns 7-9). The first column indicates the data set, the second one (n) - the number of points.

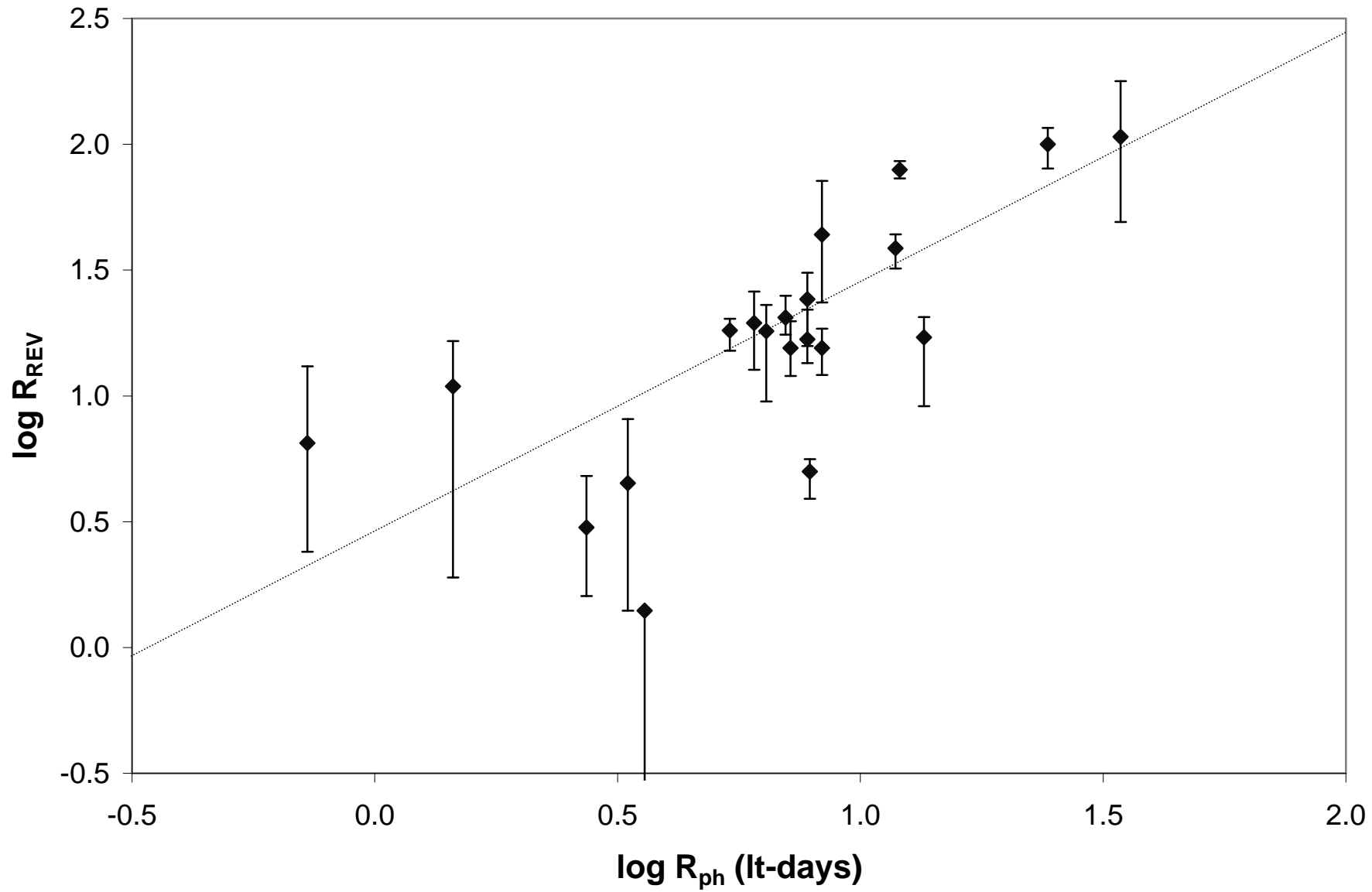
Data set	$n$ (2)	$\bar{M}_7$ (3)	$\chi^2(\bar{M})$ (4)	$a$ (5)	$\chi^2(-2x + a)$ (6)	$b$ (7)	$a$ (8)	$\chi^2(-bx + a)$ (9)
All lines, H $\beta$ 89-96	14	6.1	1.09(0.35)	8.85	2.10(0.04)	-2.05 $\pm$ 0.13	8.85 $\pm$ 0.49	1.78(0.05)
All lines, H $\beta$ 89	9	5.5	0.92(0.49)	8.58	1.57(0.15)	-1.98 $\pm$ 0.13	8.50 $\pm$ 0.51	1.22(0.29)
All lines, H $\beta$ average	9	6.0	0.87(0.51)	8.62	1.44(0.19)	-2.22 $\pm$ 0.18	9.51 $\pm$ 0.69	0.96(0.45)
H $\beta$ 89-96, centroid	6	6.6	1.72(0.15)	8.66	3.51(0.01)	-0.76 $\pm$ 0.39	4.06 $\pm$ 1.43	0.93(0.45)
H $\beta$ 89-96, peak	6	6.6	0.58(0.68)	8.66	1.67(0.15)	-1.47 $\pm$ 0.27	6.67 $\pm$ 1.00	0.66(0.62)

# NGC 5548 - various lines









# Mass-Luminosity relation

